An information-theoretic approach to designing the plane spacing for multifocal plane microscopy

Amir Tahmasbi[a,b], Sripad Ram[c], Jerry Chao[a,b], Anish V. Abraham[a,b], E. Sally Ward[b,d], and Raimund J. Ober[a,b]

[a]Dept. of Biomedical Engineering, Texas A&M University, College Station, TX, USA;
[b]Dept. of Molecular and Cellular Medicine, Texas A&M Health Science Center, College Station, TX, USA;
[c]Dept. of Immunology, University of Texas Southwestern Medical Center, Dallas, TX, USA;
[d]Dept. of Microbial Pathogenesis and Immunology, Texas A&M Health Science Center, College Station, TX, USA

ABSTRACT

Multifocal plane microscopy (MUM) is a 3D imaging modality which enables the localization and tracking of single molecules at high spatial and temporal resolution by simultaneously imaging distinct focal planes within the sample. MUM overcomes the depth discrimination problem of conventional microscopy and allows high accuracy localization of a single molecule in 3D along the z-axis. An important question in the design of MUM experiments concerns the appropriate number of focal planes and their spacings to achieve the best possible 3D localization accuracy along the z-axis. Ideally, it is desired to obtain a 3D localization accuracy that is uniform over a large depth and has small numerical values, which guarantee that the single molecule is continuously detectable. Here, we address this concern by developing a plane spacing design strategy based on the Fisher information. In particular, we analyze the Fisher information matrix for the 3D localization problem along the z-axis and propose spacing scenarios termed the strong coupling and the weak coupling spacings, which provide appropriate 3D localization accuracies. Using these spacing scenarios, we investigate the detectability of the single molecule along the z-axis and study the effect of changing the number of focal planes on the 3D localization accuracy. We further review a software module we recently introduced, the MUMDesignTool, that helps to design the plane spacings for a MUM setup.

Keywords: Cramér-Rao lower bound, Fisher Information Matrix, Single molecule microscopy

1. INTRODUCTION

High accuracy determination of the 3D positions of highly dynamic objects imaged by a fluorescence microscope is of significant practical importance as it holds the promise to provide new insights into subcellular processes and structures (see e.g.[1,2]). In particular, 3D single molecule tracking[1,3] and localization-based 3D superresolution microscopy,[4] which are the two well-known applications of single molecule fluorescence microscopy, primarily relay on the accurate estimation of the 3D location of single molecules.[5,6] However, conventional fluorescence microscopy fails to provide sufficient information about the axial location of a single molecule, especially, when it is located at or near the plane of focus.[1,3,5] This is sometimes referred to as the depth discrimination problem of conventional microscopy.[7]

To overcome the depth discrimination problem, a number of approaches have been proposed in the literature which are essentially based on modifications to the conventional microscopy setup. Examples for such approaches include engineered point spread functions (PSFs),[8] astigmatic optics,[9] interferometric optics[10] and multifocal plane microscopy (MUM).[11] A central question in the design of imaging experiments using any of the aforementioned 3D imaging modalities concerns the best possible accuracy with which the 3D location of a single molecule can be estimated as it moves along the z-axis (i.e. the optical axis). It is ideally desired to achieve

Send correspondence to Raimund J. Ober, E-mail: raimund.ober@tamu.edu

Three-Dimensional and Multidimensional Microscopy: Image Acquisition and Processing XXII, edited by Thomas G. Brown, Carol J. Cogswell, Tony Wilson, Proc. of SPIE Vol. 9330, 933011 · © 2015 SPIE · CCC code: 1605-7422/15/$18 · doi: 10.1117/12.2076769

a 3D localization accuracy that is uniform over a large depth and has small numerical values, which guarantee that the single molecule is continuously detectable.[12]

Here, we are particularly interested in MUM which provides high spatial and temporal resolution for the localization and tracking of single molecules by simultaneously imaging different focal planes within the sample.[1,11,12] In MUM, the best possible 3D localization accuracy along the z-axis is primarily controlled by the number of focal planes and their spacings.[1,12] A large number of appropriately spaced focal planes can potentially cover a large depth for viewing and tracking the particles. Fluorescence microscopy, however, is photon-limited which implies that, regardless of the number of focal planes, only a specific and limited number of photons can be collected from the sample per acquisition.[13,14] Increasing the number of focal planes splits this fixed number of photons among a larger number of planes which, in turn, leads to a less photon budget for each focal plane.[1] A poorer localization accuracy may therefore be achieved when using a large number of focal planes. Additionally, altering the spacings between the focal planes changes the image profiles of the object at the focal planes, which has two notable consequences. First, the localization accuracy of the object will be affected as it moves along the z-axis.[7] Second, the particle may become difficult to detect in the acquired image.[12] As such, for a given MUM setup the choice of the plane spacing determines whether an object can be localized with a consistent level of accuracy and whether it can be continuously detected in the image, as it moves along the z-axis.

In this paper, we address the above concerns by developing a plane spacing design strategy based on the Fisher information matrix (FIM). The FIM represents the amount of information the data provides about an unknown parameter,[14,15] e.g. the 3D location of a single molecule, and is closely related to the inverse of the best possible localization accuracy.[13,16] We particularly study the behavior of the FIM along the z-axis and introduce two spacing scenarios, the *strong coupling spacing* and the *weak coupling spacing*, which provide appropriate 3D localization accuracies. Using these spacing scenarios, we investigate the effect of the number of focal planes on the localization accuracy and comment on the detectability of the particle along the z-axis. We also briefly describe the MUMDesignTool,[12] which is a user-friendly software package developed for designing the focal plane spacing for a MUM setup.

We would like to note that the material presented here comprises a subset of the content of our recently published journal article,[12] in which detailed analyses and extensive discussions can be found.

2. PROBLEM FORMULATION AND THEORY

2.1 Fisher Information Matrix for a MUM Setup

In this section, we briefly review the concepts concerning the FIM for a MUM setup as they are necessary for the determination of the best possible 3D localization accuracy along the z-axis. Let $\Theta \subseteq \mathbb{R}^3$ be an open parameter space and let $\boldsymbol{\theta} := (x_0, y_0, z_0) \in \Theta$ be the parameter-vector of interest representing the 3D location of an object, e.g. a single molecule, in the object space with respect to the design focal plane, that is the standard infinity-corrected focal plane in conventional single plane microscopy. The best possible accuracy (standard deviation) with which the location of the single molecule can be estimated, observing its pixelated image, is given by the practical localization accuracy measure (PLAM).[12,13,17] We refer to the best possible accuracy for estimating the x, y and z coordinates of the single molecule as x_0-PLAM, y_0-PLAM and z_0-PLAM (axial-PLAM), respectively. The PLAM is determined using the Cramér-Rao lower bound (CRLB).[13,16] According to the Cramér-Rao inequality,[14,15] the covariance matrix of any unbiased estimator $\hat{\boldsymbol{\theta}}$ of a parameter-vector $\boldsymbol{\theta} \in \Theta$ is bounded from below by the inverse FIM, i.e. $\mathrm{cov}(\hat{\boldsymbol{\theta}}) \geq \boldsymbol{I}^{-1}(\boldsymbol{\theta})$. For the current 3D localization problem, the FIM $\boldsymbol{I}(\boldsymbol{\theta})$ for any given focal plane or for the MUM setup is a 3×3 matrix. The main diagonal elements of this 3×3 matrix provide information about the x, y and z coordinates of the single molecule and we denote them by x_0-FIM, y_0-FIM and z_0-FIM (axial-FIM), respectively.[12] Therefore, the x_0-PLAM, y_0-PLAM and z_0-PLAM are given by the square root of the inverse of x_0-FIM, y_0-FIM and z_0-FIM, respectively.

Suppose a pixelated detector $\{\mathcal{C}_1, \ldots, \mathcal{C}_{K_{pix}}\}$ consisting of K_{pix} pixels, where $\mathcal{C}_k \subseteq \mathbb{R}^2$, $k = 1, \ldots, K_{pix}$, denotes the area occupied by the k^{th} pixel. Assume that the pixels are mutually disjoint and postulate that we have K_{pln} focal planes where the first plane is equivalent to the design focal plane. It has been previously shown

that the photon counts detected by the pixels of the n^{th} plane due to a single molecule axially located at z_0 are realizations of independent Poisson random variables with expected values[13,14]

$$\mu_{\theta,n}(k) := \frac{N_n}{M_n^2}\int_{\mathcal{C}_{k,n}} q_{z_0-\Delta z_{1n}}\left(\frac{x}{M_n}-x_0,\frac{y}{M_n}-y_0\right)dxdy, \qquad \boldsymbol{\theta}\in\Theta,\ n=1,\ldots,K_{pln},\ k=1,\ldots,K_{pix}, \quad (1)$$

where N_n is the expected number of detected photons on the n^{th} infinite detector plane (i.e. $\mathbb{R}^2$) due to the single molecule such that $\sum_{n=1}^{K_{pln}} N_n = N_{tot}$, with N_{tot} denoting the total number of detected photons due to the single molecule on an arbitrarily positioned infinite detector plane. We note that N_{tot} is independent of the number of focal planes. The term $\mathcal{C}_{k,n}$ denotes the k^{th} pixel at the n^{th} focal plane. In addition, M_n and Δz_{1n} denote the lateral magnification at the n^{th} focal plane and the distance between the design focal plane and the n^{th} focal plane in the object space (with $\Delta z_{11}=0$), respectively, and q_{z_0} is known as the image function.[1,13]

The image function describes the image of a stationary single molecule on the detector at unit lateral magnification when the single molecule is located on the z-axis in the object space. We assume that the image function is given by the Born and Wolf 3D PSF.[1,18] It has been previously shown, under geometrical optics, that the lateral magnification for a focal plane that is shifted by a distance of Δz_{1n} from the design focal plane is given by[12,13]

$$M_n := M(\Delta z_{1n}) = M_1\frac{L-\frac{LM_1^2\Delta z_{1n}}{n_{oil}L+M_1^2\Delta z_{1n}}}{L}, \quad n=1,\ldots,K_{pln},\ \Delta z_{1n}\in\mathbb{R},$$

where n_{oil} is the refractive index of the immersion oil and L is the tube length of the microscope.

The expression of the FIM for the parameter-vector $\boldsymbol{\theta}$ at the n^{th} focal plane for a practical microscopy setup, where the acquired data is corrupted by extraneous noise, is given by[13,14,19]

$$\boldsymbol{I}_n(\boldsymbol{\theta}) = \sum_{k=1}^{K_{pix}}\frac{\psi_n(k)}{\nu_{\theta,n}(k)}\left(\frac{\partial\mu_{\theta,n}(k)}{\partial\boldsymbol{\theta}}\right)^T\frac{\partial\mu_{\theta,n}(k)}{\partial\boldsymbol{\theta}}, \qquad \boldsymbol{\theta}\in\Theta,\ n=1,\ldots,K_{pln}, \quad (2)$$

where $\nu_{\theta,n}(k)=\mu_{\theta,n}(k)+b_{k,n}$ with $b_{k,n},\ k=1,\ldots,K_{pix},\ n=1,\ldots,K_{pln}$, denoting the photon count due to the background noise at pixel $\mathcal{C}_k$ and plane n. The term $\psi_n(k)$ is known as the noise coefficient that depends on the type of detector.[19] In the absence of readout noise, $\psi_n(k)=1$ for all $k=1,\ldots,K_{pix},\ n=1,\ldots,K_{pln}$.[13] In the presence of readout noise and when using charge coupled device (CCD) and complementary metal oxide semiconductor (CMOS) detectors, the noise coefficient is given by[13]

$$\psi_n(k)=\nu_{\theta,n}(k)\times\left(\frac{e^{-\nu_{\theta,n}(k)}}{\sqrt{2\pi}\sigma_{k,n}}\int_{\mathbb{R}}\frac{\left(\sum_{l=1}^{\infty}\frac{\nu_{\theta,n}^{l-1}(k)}{(l-1)!}e^{\frac{-(z-l-\eta_{k,n})^2}{2\sigma_{k,n}^2}}\right)^2}{\sum_{l=0}^{\infty}\frac{\nu_{\theta,n}^{l}(k)}{l!}e^{\frac{-(z-l-\eta_{k,n})^2}{2\sigma_{k,n}^2}}}dz-1\right),$$

where $\eta_{k,n}$ and $\sigma_{k,n}^2$ denote the mean and the variance of the readout noise, respectively, for $k=1,\ldots,K_{pix}$ and $n=1,\ldots,K_{pln}$. The expression of the noise coefficient in the presence of stochastic signal amplification and readout noise, which are associated with an electron-multiplying CCD (EMCCD) detector, can be found in.[19]

Since the data acquisition in each focal plane is independent of the data acquisition in the other planes, the FIM for a MUM setup is simply the sum of the FIMs of the individual focal planes[1,12] and we have

$$\boldsymbol{I}_{MUM}(\boldsymbol{\theta}) = \boldsymbol{I}_1(\boldsymbol{\theta})+\boldsymbol{I}_2(\boldsymbol{\theta})+\cdots+\boldsymbol{I}_{K_{pln}}(\boldsymbol{\theta}), \qquad \boldsymbol{\theta}\in\Theta\subseteq\mathbb{R}^3. \quad (3)$$

As we will discuss in the next section, this additive property of the FIMs makes it very convenient to define the focal plane spacing problem in terms of the FIMs rather than directly in terms of the PLAMs.

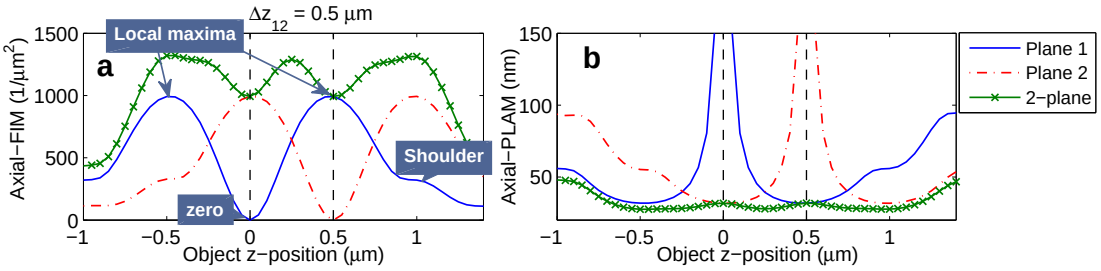

Figure 1. The axial-FIM and the axial-PLAM for conventional single plane microscopy and MUM. (a) The axial-FIM and (b) the axial-PLAM for a 2-plane MUM setup and two conventional single plane setups (Plane 1 and Plane 2) as a function of the z-position of the single molecule. The zero, local maxima and shoulders of the axial-FIM of Plane 1 are marked in panel (a). The results are calculated for a 100x, NA 1.3 objective lens. The plane spacing (Δz_{12}) is 0.5 μm, the photon count is 250 photons/plane and the emission wavelength is 520 nm. The background level is 1 photon/pixel/plane and the standard deviation of the readout noise is 2 e^-/pixel. The ROI size is 11 $\times$ 11 pixels.

2.2 Graphical Interpretation of the Plane Spacing Design Strategy

In this section, we give a graphical interpretation for the design of the focal plane spacing for a MUM setup. To this end, we first study the behavior of the axial-FIM and the axial-PLAM along the z-axis for both a conventional microscopy setup and a MUM setup. Figure 1(a) shows the axial-FIM for a conventional single plane microscopy setup with a design focal plane as a function of the z-position of the single molecule ("Plane 1"), computed using Eq. 2. It is clear that the axial-FIM for this focal plane is zero when the object is at the focal plane, which implies that the data does not provide any information about the z-location of the point source; we refer to this spot as the *zero* of the axial-FIM. A consequence of the zero of the axial-FIM is the depth discrimination problem, illustrated in Fig. 1(b) ("Plane 1"), where the axial-PLAM for the design focal plane increases without bound as the single molecule approaches Plane 1. This corresponds to a high uncertainty in estimating the z-position of the single molecule when it is located near the plane of focus.[1,7] As the single molecule moves away from the focal plane, the axial-FIM increases and at some z-position it reaches a peak which we refer to as the *local maximum* of the axial-FIM. Further moving the single molecule away from the focal plane gradually decreases the axial-FIM and at some z-position the axial-FIM has a bump which we refer to as the *shoulder* of the axial-FIM. The described behavior of the axial-FIM is symmetric with respect to the z-position of the focal plane obviously due to the axial symmetry of the Born and Wolf 3D PSF.[18]

Figure 1(b) also shows the axial-PLAM for a 2-plane MUM setup along the z-axis. For brevity, we refer to this and its corresponding axial-FIM as axial-PLAM$_{MUM}$ and axial-FIM$_{MUM}$, respectively. As can be seen, the axial-PLAM$_{MUM}$ is relatively constant along the z-axis including at the focal planes when compared to the axial-PLAM for a conventional microscope (i.e. "Plane 1"). The flatness of axial-PLAM$_{MUM}$ curve depends on the plane spacing and our ultimate design objective is to obtain an appropriate level of the axial-PLAM$_{MUM}$. Due to the fact that the PLAM$_{MUM}$ is specified in terms of the inverse of the FIM$_{MUM}$, minimizing the axial-PLAM$_{MUM}$ is closely related to maximizing the axial-FIM$_{MUM}$ (see Section 2.1). We therefore carry out the main steps of the focal plane spacing design by investigating the axial-FIM as this will prove to be a convenient criterion due to two important properties of the axial-FIM. First, as pointed out earlier, the axial-FIM$_{MUM}$ is the sum of the axial-FIMs for the individual focal planes.[1] Hence, as shown in Fig. 1(a), the axial-FIM$_{MUM}$ curve along the z-axis is obtained by adding the axial-FIM curves of the individual focal planes. The second important property of the axial-FIM is that, to a good approximation, the graphs of axial-FIMs of the different focal planes are simply translated versions of the graph of the axial-FIM for the design focal plane along the z-axis (see Fig. 1(a)).[12] We note that this property is based on the assumption that different focal planes have similar experimental conditions, e.g. the photon count and extraneous noise, as would be the case if identical detectors are used and the emission light is equally split among the detectors for the different planes. The second property in particular implies that changing the position of a focal plane with respect to the other planes amounts to a corresponding translation of the graph of the axial-FIM.

These two properties provide the basis for a graphical interpretation of the design process for focal plane

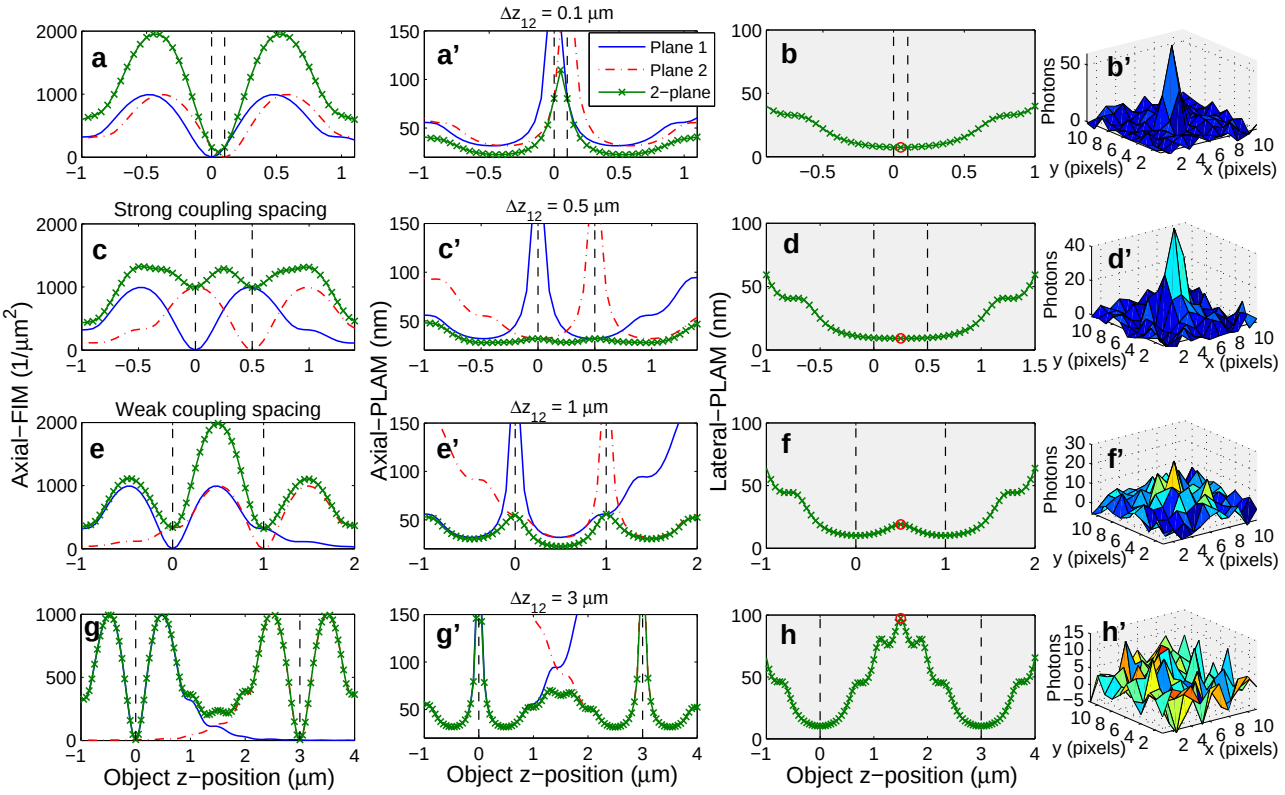

Figure 2. The effect of plane spacing on the axial-FIM, the axial-PLAM and the lateral-PLAM for a MUM setup. Panels (a), (c), (e) and (g) ((a'), (c'), (e') and (g')) show the axial-FIM (axial-PLAM) for a 2-plane MUM setup as a function of the z-position of the point source for different plane spacings. The figure also shows the axial-FIMs and axial-PLAMs of focal planes 1 and 2. Panels (b), (d), (f) and (h) show the corresponding lateral-PLAMs for the MUM setup. Panels (b'), (d'), (f') and (h') show the mesh plots of the simulated images of single molecules located at z-positions shown by the red circles on the design plane. The plane spacings (Δz_{12}) are 0.1, 0.5, 1 and 3 μm from top to bottom. Panels (c), (c'), (d) and (d') are associated with the strong coupling spacing whereas panels (e), (e'), (f) and (f') correspond to the weak coupling spacing. The results are calculated for a 100x, NA 1.3 oil immersion objective lens where the photon count is 250 photons/plane and the emission wavelength is 520 nm. The background level is 1 photon/pixel/plane and the standard deviation of the readout noise is 2 e^-/pixel. The ROI size is 11 $\times$ 11 pixels. The vertical dashed lines show the position of focal planes.

spacing. The design process can therefore be thought of as shifting the graphs of the axial-FIMs such that their sum, i.e. the axial-FIM$_{MUM}$, has the desired values for the range of z-positions that are of interest.

3. RESULTS

3.1 Strong and Weak Coupling Spacings: Constant Axial-PLAM

The primary requirement in the design of MUM experiments is to obtain a constant axial-PLAM$_{MUM}$ along the z-axis. A constant axial-PLAM$_{MUM}$ allows estimating the axial location of a single molecule with a constant level of accuracy across the desired depth. As such, as a first step we investigate the influence of changing the plane spacings on the axial-PLAM$_{MUM}$ for a 2-plane MUM setup. We defer the study of MUM setups with more than two focal planes to the subsequent sections. The behavior of the axial-PLAM of a 2-plane MUM setup for different plane spacings is illustrated in Figs. 2(a'), (c'), (e') and (g'), where it is shown that changing the plane spacing changes the flatness of the curve. For a small plane spacing ($\Delta z_{12} = 0.1$ μm), there is a significant variation in the axial-PLAM$_{MUM}$ value between the focal planes, i.e. the axial-PLAM$_{MUM}$ varies from 22 nm to 110 nm over the z-range of [-0.6, 1.1] μm (see Fig. 2(a')).

Increasing the plane spacing, improves the flatness of axial-PLAM$_{MUM}$ curve and, as can be seen in Fig. 2(c'), a certain spacing ($\Delta z_{12} = 0.5$ μm) yields a relatively flat curve. For this spacing, the axial-PLAM$_{MUM}$ varies only from 28 nm to 31 nm over the same z-range of [-0.6, 1.1] μm. This relatively constant axial-PLAM$_{MUM}$ is obtained when the local maximum of the axial-FIM of the second plane overlaps with the zero of the axial-FIM of the first plane (see Fig. 2(c)). We refer to this spacing as the strong coupling spacing. Further increasing the plane spacing worsens the flatness of the curve (see Fig. 2(e')). Hence, we set the largest acceptable plane spacing to be the case where the shoulder of the axial-FIM of the second plane overlaps with the zero of that of the first plane (see Figs. 2(e)). We refer to this spacing as the weak coupling spacing. For this spacing, the axial-PLAM$_{MUM}$ varies from 23 nm to 54 nm over the z-range of [-0.6, 1.1] μm, as can be seen in Fig. 2(e).

A very large plane spacing ($\Delta z_{12} = 3$ μm) results in large fluctuations in the curve, with large axial-PLAM$_{MUM}$ values both between the focal planes and at the focal planes (see Fig. 2(g')). This is primarily due to the fact that the axial-FIMs of two distantly spaced focal planes make small contributions to the axial-FIM$_{MUM}$ at the focal planes (see Fig. 2(g)) and, as such, the axial-PLAM$_{MUM}$ at each focal plane is large.

3.2 Constant Lateral-PLAM and Detectability of the Particle

In addition to a constant z-localization accuracy along the z-axis, obtaining constant x- and y-localization accuracy is also of importance, especially, in the context of 3D tracking. In this section, we analyze the behavior of the x_0-PLAM and y_0-PLAM for a MUM setup along the z-axis. To this end, we define the lateral-PLAM as follows[12]

$$\text{Lateral-PLAM} := \left((x_0\text{-PLAM}_{MUM})^2 + (y_0\text{-PLAM}_{MUM})^2\right)^{1/2}.$$

The lateral-PLAM quantifies the best possible accuracy for the lateral localization of a particle. A large value for the lateral-PLAM at a certain z-position predicts a poor lateral localization accuracy at that z-position. Importantly, a poor lateral localization accuracy can also be interpreted as high uncertainty in visually detecting the particle in the acquired image.[12]

Figures 2(b), (d), (f) and (h) show the lateral-PLAM for a 2-plane MUM setup for different plane spacings, which corresponds to the axial-PLAM described in the previous section. When the focal planes are located close to one another ($\Delta z_{12} = 0.1$ μm), the lateral-PLAM varies from 7.3 nm to 32.6 nm over the z-range of [-0.3, 0.8] μm (see Fig. 2(b)). For this plane spacing, the numerical value of the lateral-PLAM at the midpoint between the focal planes is relatively small, i.e. 7.3 nm. Correspondingly, the point source can be clearly visually identified in a MUM image as shown in the mesh plot (Fig. 2(b'), where only the image from the first focal plane is shown).

Adjusting the plane spacing based on the strong coupling spacing (Fig. 2(d)) and the weak coupling spacing (Fig. 2(f)) provides relatively constant lateral-PLAMs. More specifically, for the strong coupling spacing the lateral-PLAM varies from 9.2 nm to 13.7 nm over the z-range of [-0.3, 0.8] μm, whereas for the weak coupling spacing it varies from 10.1 nm to 19 nm over the same z-range. For a large plane spacing ($\Delta z_{12} = 3$ μm), the lateral-PLAM varies significantly, i.e. from 10.3 nm to 45.1 nm, over the same z-range (see Fig. 2(h)). This implies that the lateral location of the particle cannot be estimated with a constant level of accuracy.

From a detectability perspective, as the plane spacing increases, the numerical value of the lateral-PLAM varies significantly such that at a certain plane spacing the point source becomes barely detectable in the image. For example, for a plane spacing of 1 μm that corresponds to the weak coupling spacing, the lateral-PLAM for a point source at $z = 0.5$ μm is 19 nm and at this position the particle is marginally visible in the image (see Fig. 2(f')). For larger plane spacings the particle can no longer be identified in the image (Fig. 2(h')). This is due to the fact that as the plane spacing increases, for certain z-positions (especially near the midpoint between the focal planes), the distance between the particle and each focal plane becomes so large that the particle is significantly out of focus and is therefore undetectable in the image.

The above discussion suggests that the weak coupling scenario provides a guideline for adjusting the plane spacing to achieve a large viewing range and helps in designing MUM setups, for example, to observe a particular cellular process that occurs over a large z-range.

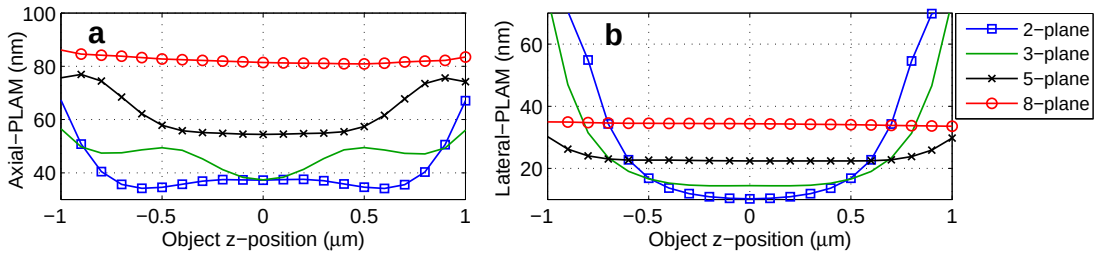

Figure 3. The effect of changing the number of focal planes on the 3D localization accuracy. (a) The axial-PLAM and (b) the lateral-PLAM for a MUM setup with different numbers of focal planes over a range of [-1, 1] μm. The magnification, the numerical aperture, emission wavelength, and the ROI size are 100x, 1.3, 520 nm, and 11×11 pixels, respectively. The focal planes are located based on the strong coupling spacing. The total photon count is 1000 photons and is split equally among the focal planes. The background level and the standard deviation of the readout noise are 25 photons/pixel/plane and 8 e^-/pixel, respectively.

3.3 Appropriate Number of Focal Planes

As mentioned earlier, the second important question in the design of MUM experiments concerns the appropriate number of focal planes that are required to cover a sample of a certain thickness.[1,12] This section is devoted to addressing this concern by studying the effect of changing the number of focal planes on the 3D localization accuracy of a MUM setup along the z-axis. The axial-PLAMs for MUM setups with 2 to 8 focal planes over the range of [-1, 1] μm are displayed in Fig 3(a), where the planes are placed based on the strong coupling spacing. As it is the case in practice, we assume that the total photon count is fixed and is equally split among the focal planes. Fig. 3(a) shows that the axial-PLAM of the 2-plane setup has relatively small numerical values along the z-axis. However, the values vary significantly (e.g. they vary from 34 nm to 67 nm over the z-range of [-1, 1] μm). Increasing the number of planes from 2 to 3, elevates the numerical values of the axial-PLAM$_{MUM}$ while the curve becomes more flat (i.e. the axial-PLAM$_{MUM}$ varies from 37 nm to 56 nm over the same z-range).

Further increasing the number of focal planes, e.g. to 5 or 8, provides more flat axial-PLAM$_{MUM}$ curves along the z-axis. For instance, for an 8-plane setup the axial-PLAM values vary only from 81 nm to 86 nm over the same z-range. However, the numerical value of the axial-PLAM for a MUM setup with a large number of planes is consistently greater than that for a MUM setup with a small number of planes. A consistently large axial-PLAM$_{MUM}$ value implies a poor localization accuracy along the z-axis. The effect of changing the number of focal planes on the lateral-PLAM is analogous to its effect on the axial-PLAM$_{MUM}$ (see Figure 3(b)).

Consequently, the practical implication of this behavior is that we can achieve a relatively constant 3D localization accuracy across the desired depth by increasing the number of focal planes. Nevertheless, as the number of focal planes increases, the numerical values of the localization accuracy become consistently large along the z-axis. The rationale for this behavior is that placing a large number of focal planes, splits the emitted light from the sample among the planes such that the number of photons detected from the sample at each plane becomes relatively small when compared to the readout noise. This results in large numerical values in the axial-PLAM$_{MUM}$ and the lateral-PLAM which depend on the number of detected photons per focal plane.[1,12]

4. THE MUMDESIGNTOOL

To facilitate and speed up the tedious and time-consuming process of designing the focal plane spacing for a MUM setup, we developed a new software module, the MUMDesignTool*,[12] which is incorporated with the recent release of our previously developed FandPLimitTool†.[17] The MUMDesignTool is developed in the MATLAB environment based on an object-oriented programming methodology and provides a user-friendly graphical user interface (see Fig. 4). Powered by two main working modes termed the *rapid mode* and the *precise mode*, the MUMDesignTool is capable of computing and plotting the 3D localization accuracy for MUM setups with up to

*The software package is available on-line at http://www.wardoberlab.com/software/mumdesigntool/.
†For more information visit http://www.wardoberlab.com/software/fandplimittool/.

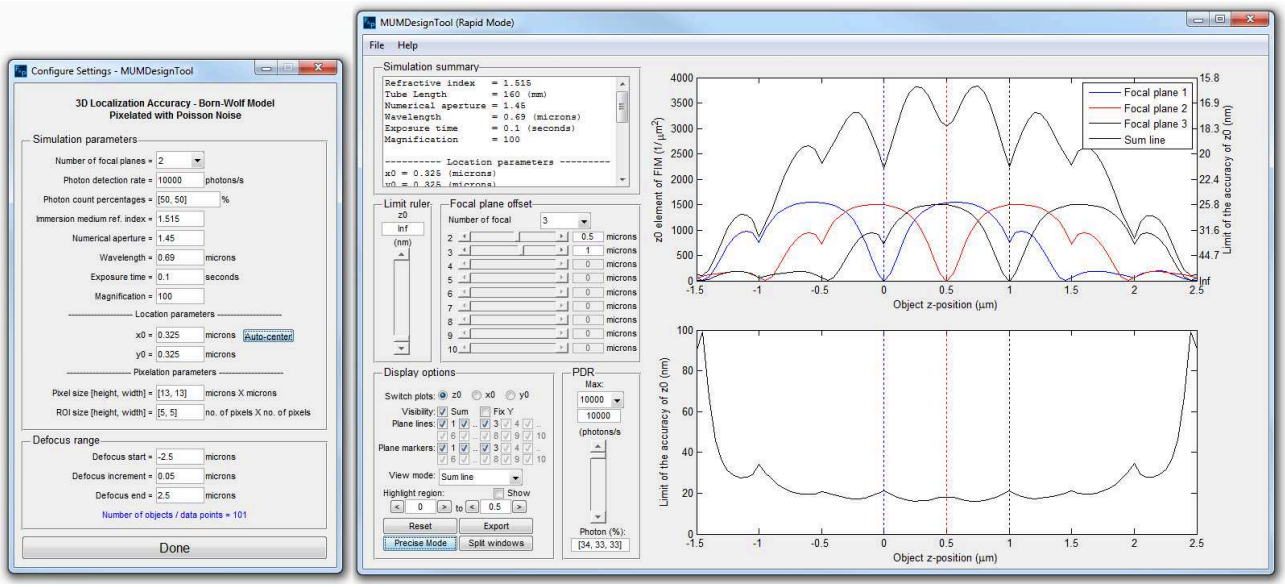

Figure 4. The graphical user interface of the MUMDesignTool. The left and right panels show the configure settings and the rapid mode windows of the MUMDesignTool.

10 focal planes. In particular, the rapid mode allows the fast calculation of the 3D localization accuracy for a MUM setup by making use of an approximate but fast approach explained in detail in.[12] The main assumptions for the rapid mode are that the lateral magnification is constant at different focal planes and that the data is devoid of extraneous noise sources. The precise mode, on the other hand, calculates the 3D localization accuracy without any approximation (i.e. this mode directly computes Eq. 3).

The recommended procedure to designing the plane spacing using this package is to first use the rapid mode to interactively change the plane spacing and the number of planes and visualize the behavior of the PLAM. This helps to find a candidate spacing based on one of the introduced spacing scenarios. The next step is then to run the precise mode with the extraneous noise parameters, and the candidate spacing to verify that the designed spacings are appropriate in the presence of noise. If there is a significant discrepancy between the results of the rapid mode and the results of the precise mode, the plane spacing designed using the rapid mode (i.e. the candidate spacing) should be fine tuned. The fine tuning can be performed by slightly increasing and/or decreasing the candidate spacing and then rerunning the precise mode. The results of the precise mode for these slightly different spacings can then be compared to find the desired spacing.

ACKNOWLEDGMENTS

This work was supported in part by the National Institutes of Health (R01 GM085575).

REFERENCES

1. Ram, S., Prabhat, P., Chao, J., Ward, E. S., and Ober, R. J., "High accuracy 3d quantum dot tracking with multifocal plane microscopy for the study of fast intracellular dynamics in live cells," *Biophys. J.* **95**, 6025–6043 (2008).
2. Dehmelt, L. and Bastiaens, P. I. H., "Spatial organization of intracellular communication: insights from imaging," *Nature Rev. Mol. Cell Biol.* **11**, 440–452 (2010).
3. Dalgarno, P. A., Dalgarno, H. I. C., Putoud, A., Lambert, R., Paterson, L., Logan, D. C., Towers, D. P., Warburton, R. J., and Greenaway, A. H., "Multiplane imaging and three dimensional nanoscale particle tracking in biological microscopy," *Opt. Express* **18**, 877–884 (2010).

4. Betzig, E., Patterson, G. H., Sougrat, R., Lindwasser, O. W., Olenych, S., Bonifacino, J. S., Davidson, M. W., Lippincott-Schwartz, J., and Hess, H. F., "Imaging intracellular fluorescent proteins at nanometer resolution," *Science* **313**, 1642–1645 (2006).
5. Ober, R. J., Tahmasbi, A., Ram, S., Lin, Z., and Ward, E. S., "Quantitative aspects of single molecule microscopy: Information-theoretic analysis of single-molecule data," *IEEE Signal Process. Mag.* **32**, 58–69 (2015).
6. Deschout, H., Zanacchi, F. C., Mlodzianoski, M., Diaspro, A., Bewersdorf, J., Hess, S. T., and Braeckmans, K., "Precisely and accurately localizing single emitters in fluorescence microscopy," *Nat. Methods* **11**, 253–266 (2014).
7. Ram, S., Ward, E. S., and Ober, R. J., "How accurately can a single molecule be localized in three dimensions using a fluorescence microscopy?," *Proc. SPIE* **5699**, 426–435 (2005).
8. Pavani, S. R. P. and Piestun, R., "Three dimensional tracking of fluorescent microparticles using a photon-limited double-helix response system," *Opt. Express* **16**, 22048–22057 (2008).
9. Kao, H. P. and Verkman, A. S., "Tracking of single fluorescent particles in three dimensions: use of cylindrical optics to encode particle position," *Biophys. J.* **67**, 1291–1300 (1994).
10. Shtengel, G., Galbraith, J. A., Galbraith, C. G., Lippincott-Schwartz, J., Gillette, J. M., Manley, S., Sougrat, R., Waterman, C. M., Kanchanawong, P., Davidson, M. W., Fetter, R. D., and Hess, H. F., "Interferometric fluorescent super-resolution microscopy resolves 3d cellular ultrastructure," *Proc. Natl. Acad. Sci. USA* **106**, 3125–3130 (2009).
11. Prabhat, P., Ram, S., Ward, E. S., and Ober, R. J., "Simultaneous imaging of different focal planes in fluorescence microscopy for the study of cellular dynamics in three dimensions," *IEEE Trans. Nanobiosci.* **3**, 237–242 (2004).
12. Tahmasbi, A., Ram, S., Chao, J., Abraham, A. V., Tang, F. W., Ward, E. S., and Ober, R. J., "Designing the focal plane spacing for multifocal plane microscopy," *Opt. Express* **22**, 16706–16721 (2014).
13. Ober, R. J., Ram, S., and Ward, E. S., "Localization accuracy in single-molecule microscopy," *Biophys. J.* **86**, 1185–1200 (2004).
14. Snyder, D. L. and Miller, M. I., [*Random Point Processes in Time and Space*], Springer Verlag, New York, USA, second ed. (1991).
15. Kay, S. M., [*Fundamentals of Statistical Signal Processing: Estimation Theory*], Prentice Hall PTR, Upper Saddle River, NJ, first ed. (1993).
16. Ram, S., Ward, E. S., and Ober, R. J., "A stochastic analysis of performance limits for optical microscopes," *Multidim. Sys. Sig. Proc.* **17**, 27–57 (2006).
17. Abraham, A. V., Ram, S., Chao, J., Ward, E. S., and Ober, R. J., "Quantitative study of single molecule location estimation techniques," *Opt. Express* **17**, 23352–23373 (2009).
18. Born, M. and Wolf, E., [*Principles of Optics*], Cambridge University Press, Cambridge, UK, seventh ed. (2002).
19. Chao, J., Ward, E. S., and Ober, R. J., "Fisher information matrix for branching processes with application to electron-multiplying charge-coupled devices," *Multidim. Sys. Sig. Proc.* **23**, 349–379 (2012).